Appl Phys A (2009) 94: 667–674
DOI 10.1007/s00339-008-4955-7

Applied Physics A
Materials Science & Processing

Laser rapid thermal annealing of quantum semiconductor wafers: a one step bandgap engineering technique

R. Stanowski · J.J. Dubowski

Received: 13 February 2008 / Accepted: 20 October 2008 / Published online: 18 November 2008
© Springer-Verlag 2008

Abstract We report on a new Laser Rapid Thermal Annealing (Laser-RTA) technique for one-step bandgap engineering at selected areas of quantum semiconductor wafers. The technique is based on using a 150 W 980 nm fiber coupled laser diode and a 30 W TEM00 1064 nm Nd:YAG laser for background heating and 'writing', respectively, the regions of the quantum well intermixed (QWI) material. The implementation of a 3D Finite Element Method for modeling of laser induced temperature profiles allows for the design of processing schemes that are required for accurate bandgap engineering at the wafer level. We demonstrate that arbitrary shaped lines of the QWI material can be fabricated with the Laser-RTA technique in InGaAs/InGaAsP quantum well microstructures.

PACS 81.40.Tv · 78.55.Cr · 81.07.St · 68.35.Fx · 61.80.Ba · 81.16.-c

1 Introduction

Selective area bandgap engineering of quantum semiconductor heterostructures is the subject of intense investigations due to the potential of this approach in the fabrication of advanced devices and, in particular, photonic integrated circuits (PICs). The challenge is to develop a manufacturing technology capable of cost-attractive delivery of photon emitters and PICs comprising lasers, modulators, waveguides and other active photonic devices. For quantum well (QW) and quantum dot (QD) microstructures, spatially selective intermixing of the QW (QD) and barrier materials, known as quantum well (dot) intermixing (QWI/QDI), has become one of the most investigated methods for selective-area bandgap engineering [1–3]. The common QWI techniques have been based on impurity [4, 5], point defect [6], ion implantation [7], and impurity-free vacancy [8] diffusion. Additionally, transient melting of multiple layers by pulsed laser irradiation [9] has been demonstrated to be effective for QWI. Laser annealing has also been used to introduce encapsulant Si into the epitaxial layers and stimulate impurity-induced disordering [10]. Pulsed Nd:YAG laser ($\lambda = 1064$ nm) irradiation through a dedicated mask has been reported to allow carrying out the QWI process with lateral resolutions of about 25 μm [11] and 3 μm [12]. However, all conventional QWI techniques suffer from a lack of accuracy due to the difficult to control multi-step approach, which is one of the reasons limiting their industrial applications. The infrared (IR) continuous wave (CW) laser has been demonstrated to be an attractive tool for one-step QWI, yielding material that is of high electrical and optical quality [13]. Early results have indicated the feasibility of this approach for writing quantum boxes [14]. However, with the exception of a 4-line array of the QWI material demonstrated in GaAs/AlGaAs samples [15] the IR CW laser QWI technique has not been explored for industrial size wafer level processing. The need to use cryo-cooling to prevent surface damage [16] or a hot plate for background heating [11, 17] reduce the feasibility of this approach for selected site QWI of large area wafers. For instance, heating of the entire 2 inch diameter wafer with a hot plate technique would create the problem of dissipating significant amounts of power; thus the requirement of bulky and difficult to control experimental setups. To address this problem, we have

R. Stanowski · J.J. Dubowski (✉)
Department of Electrical and Computer Engineering, Center of Excellence for Information Engineering, Université de Sherbrooke, Sherbrooke, QC J1K 2R1, Canada
e-mail: jan.j.dubowski@usherbrooke.ca

developed a two-laser rapid thermal annealing (Laser-RTA) technique that allows for selected area rapid heating/cooling of semiconductor wafers.

Our preliminary 3D finite element method (FEM) calculations have indicated the feasibility of this approach for large area wafer bandgap engineering [18, 19]. Here, we report on the results of high-precision selective area QWI in GaInAs/GaInAsP microstructures and the fabrication of arbitrary shape lines of QWI material.

2 Experimental details

A schematic diagram of the experimental setup is shown in Fig. 1. It consists of two infrared laser irradiation sources. A fiber pigtailed (1 mm core, $NA = 0.22$) CW GaAs/AlGaAs laser diode (LD) operates at 980 nm and delivers power of up to 150 W. The second laser source is a CW Nd:YAG TEM00 laser operating at 1064 nm and delivering power of up to 30 W. The diameter of the LD spot on the sample can be regulated, typically, between 2 and 25 mm. The role of LD is to increase the wafer background temperature to near the QWI threshold. A galvanometric scanner (GS) allows to raster the Nd:YAG laser beam over the sample with a controlled velocity of 1–4000 mm/s. An F-Theta lens mounted at the output of the GS head assures that a beam with the same profile is delivered to any site of the wafer surface. The diameter of the Nd:YAG laser spot used in these experiments was 0.5 mm, but with a special beam delivery optics irradiation is possible with a 12 μm diameter spot. A low-resolution, custom designed IR camera (IR-CAM) with 640 × 480 pixels was used to map the semiconductor wafer temperature. The spectral region used by the IR-CAM device was set up with a narrow band filter to 820–840 nm, which is outside of the InP (∼950 nm) and the InGaAs QW (1550 nm) emission regions. The 980 and 1064 nm notch filters were additionally applied to increase the efficiency of the system and eliminate both laser lines. The IR-CAM could collect radiation from the whole 2 inch diameter wafer at the rate of 4 Hz. The minimum temperature that could be monitored with this instrument was about 350°C. Temperature measurements of the Nd:YAG laser irradiated spots were carried out with a 2-channel fiber optic pyrometer (MIKRON M680) designed for collecting radiation from circular areas of 0.4 and 0.7 mm in diameter. Transient temperature behavior at selected spots irradiated with the laser was carried out at the rate of 10 Hz. The minimum temperature that could be monitored with the pyrometer was about 435°C. The processed samples were held in a room ambient environment. The full size wafers (2 inch diameter) were suspended on 3 quartz rods to minimize heat energy dissipation by thermal conductivity. Smaller samples were located above a 9 mm × 9 mm opening in a graphite wafer and they were backside irradiated with a 25 mm diameter LD beam.

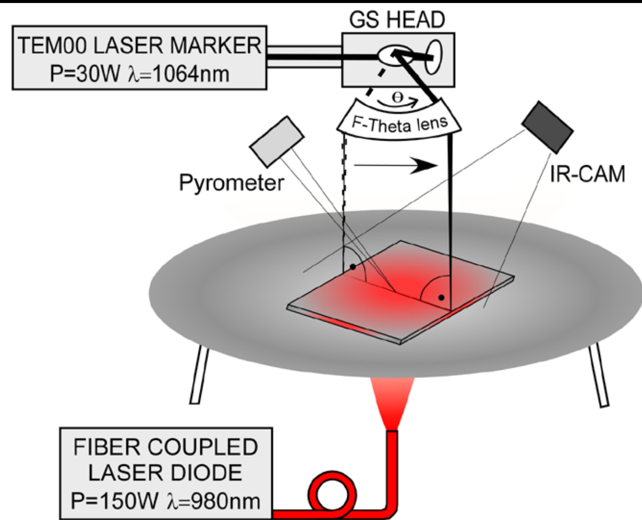

Fig. 1 Schematic diagram of the Laser Rapid Thermal Annealing setup

Room temperature photoluminescence (PL) measurements were carried out with a commercial mapper (Philips PLM-150) using an Nd:YAG laser ($\lambda = 532$ nm) as an excitation source and an InGaAs array detector. The PL mapping was carried out with a 10 μm step-resolution.

The Si wafer (sample #1) was of 2 inches in diameter and 0.5 mm thick. The InGaAsP/InP microstructure consisted of 5 QWs (6 nm thick InGaAs) and 4 barriers (10 nm thick InGaAsP) material. The topmost QW was coated with approximately 10 nm thick barrier material of InGaAsP and a 70 nm thick InP cap. Both the QWs and barriers were n-type (Si doped at 8×17 cm^{-3}). The microstructure was grown on a 0.375 mm thick InP wafer. The InGaAsP/InP samples used for studying dynamics of laser-induced temperatures (sample #2), for writing an array of parallel lines of the QWI material (sample #3) and that used for demonstrating an arbitrary shape line of the QWI material (sample #4) had dimensions of 10 mm × 14 mm. They were capped with PECVD 264 nm thick SiO_2 layers on the polished (front) side, and with 740 nm SiO_2 on the back side. The SiO_2 caps prevented the wafers from high-temperature decomposition. In addition, the top SiO_2 cap served as an antireflection coating increasing the coupling efficiency of the irradiating Nd:YAG laser beam. Optical reflection measurements carried out for InGaAsP/InP wafer at 1064 nm have shown that the reflected power decreased from 39% for a bare wafer to 3% for the wafer coated with 264 nm thick SiO_2.

3 Modeling and experimental verification of laser induced transient temperature profiles in Si and InP wafers

A FEM approximation [20] was implemented for the calculation of temporal and spatial temperature profiles induced in semiconductor wafers using commercial COMSOL software. A preliminary analysis of the irradiation conditions and the influence of material parameters on the generated temperature profiles in GaAs obtained with a stationary CW Nd:YAG laser ($\lambda = 1064$ nm) were discussed elsewhere [18]. Here we implement a more advanced 3D FEM model that includes the background heating provided by the LD source and describes the effect of the moving laser beam on achievable maximum temperatures. The FEM approach takes advantage of the finite element discretization of the calculated model's geometry into mesh elements. The properties of adjacent elements in the nodes of the generated net are shared during progressive iteration steps, so the energy flux phenomena could be calculated, e.g., for diffusion or heat transfer [20]. The FEM method allows generating mesh elements of various sizes and shapes, depending on the modeled physical process. The size of mesh elements is a critical factor for accuracy of the calculated results, but it also influences the total time of calculations. The heat balance according to the heat transfer partial differential equation, for every differential element, is based on the following relation: Heat in $-$ Heat out $=$ Heat accumulated $+$ Heat generated [21], which could be expressed by the following equation:

$$Q - \nabla(k\nabla T) = \rho Cp(\partial T/\partial t). \quad (2)$$

The formula for Q, which describes the heat source, takes into account optical reflectivity, laser beam power density, beam shape and optical absorption of the irradiated wafer. The boundary equation is given by:

$$q_0 - h(T_{\text{inf}} - T) + \varepsilon \cdot \sigma \cdot \left(T_{\text{amb}}^4 - T^4\right) = k\nabla T. \quad (3)$$

Definition of symbols describing (2) and (3) and their values used in the calculations are gathered in Table 1. The density, ρ, of InP changes less than 3% in the temperature range of interest and we assumed it to be constant. Temperature dependent specific heat Cp was included in the calculations,

Table 1 Material parameters used in FEM calculations of laser-induced temperatures in Si and InP wafers

Symbol	Definition	Value	
Q	Laser generated heat	$(1-R)\cdot I\cdot A\cdot\alpha\cdot\exp(-\alpha\cdot z)$ [W/m^3]	
I	Laser beam intensity	1064_Power/($\pi\cdot$ 1064_radius^2) [W/m^2]	
A	Laser beam shape function	$\exp(-(x^2+y^2)/(2\cdot$ 1064_ radius^2))	
q_0	Laser energy inward flux	$I\cdot A\cdot(1-R)$ [W/m^2]	
T	Wafer temperature	Calculated [K]	
z	Laser radiation penetration depth	Calculated [m]	
σ	Stefan Boltzman's constant	$5.67\cdot 10^{-8}$ [W/m^2·K^4]	
Tinf	Temperature above surface	T-50 [K]	
Tamb	Ambient temperature	296 [K]	
		Si	InP
R	Reflectivity at 1064 nm	10%	3% (SiO_2 AR)
α	Absorption of 1064 nm	1 [cm^{-1}] @$T > 77$ K 2.3 [cm^{-1}] @$T > 300$ K 2×10^3 [cm^{-1}] @$T > 676$ K [31]	1×10^{-7} [cm^{-1}] @$T > 300$ K 2.3 [cm^{-1}] @$T > 530$ K 1.5×10^5 [cm^{-1}] @$T > 775$ K 7.8×10^7 [cm^{-1}] @$T > 975$ K [26]
Cp	Specific heat	703 [J/(kg·K)]@300 K [30]	410 [J/(kg·K)] @300 K [30] 455 [J/(kg·K)] @1000 K [22]
k	Thermal conductivity	$605\cdot\exp(-T/205)+27$ [W/(m·K)] [32]	$259\cdot\exp(-T/182)+15$ [W/(m·K)] [22]
ρ	Density	2329 [kg/m^3] [30]	4810 [kg/m^3] [30]
h	Convective heat transfer	20 [W/m^2·K]	20 [W/m^2·K]
ε	Emissivity	0.7 [27]	0.7 [28]

although the weak temperature dependence of this coefficient (it changes from 410 J/kg·K at 300 K to 455 J/kg·K at 1000 K [22]) indicates that such dependence has a negligible effect on the accuracy of our calculations. The simulations showed the importance of using the temperature dependent thermal conductivity coefficient, k. Its value at 1000 K is 5 times smaller than at room temperature [22]. This results in slower heat dissipation at elevated temperatures and, consequently, in faster rates of temperature increase induced by the laser beam. After preheating the surface region to temperatures at which the semiconductor bandgap is comparable to, or smaller than the laser photon energy (approximately 500°C for InP), the bulk absorption, α, will become non-negligible. For temperatures higher than 500°C the bulk absorption of InP reaches 10^4–10^5 cm^{-1} [23, 24], which for the Nd:YAG laser corresponds to the absorption depth of 1.0–0.1 μm.

To model the Laser-RTA temperature profiles induced in InGaAsP/InP sample, we carried out calculations for a SiO_2 coated InP wafer ($\varepsilon = 0.7$). Such an approximation is quite reasonable given that the thickness of this wafer (375 μm) significantly exceeds that of the QW-barrier active region (∼70 nm). Based on available absorption data for InGaAs–InGaAsP QW heterostructures [25] and InP [26], we estimated that the overall absorption of the InP cap and a 375-μm-thick substrate at room temperature is over 300 times greater than that of the active region. Furthermore, only 0.05% of the 980 nm radiation was measured to be absorbed at this temperature by the investigated heterostructures. The InP absorption increases exponentially to 9×10^5 and 2.3×10^6 cm^{-1} at 550 and 750°C, respectively. Thus, it is reasonable to assume that the heating of the investigated microstructures occurs primarily due to absorption of the laser radiation in InP.

By solving (2) and (3), it is possible to describe temporal and spatial temperature profiles induced by both LD and Nd:YAG laser sources at any point of the wafer. Figure 2 shows transient temperature behavior at the center of the Si (sample #1) and InP (sample #2) wafers irradiated with LD and Nd:YAG sources. Backside irradiation of the Si wafer with the 61 W LD, as shown by the experimental results (solid line), allows to achieve a steady temperature of about 515°C within approximately 25 s from the onset of the irradiation. Additional irradiation with the 1.2 W Nd:YAG laser at the 58th second of the experiment results in a rapid increase of the temperature to 555°C. This temperature transition is achieved in about 5 s. Conversely, the rate at which wafer temperature decreases, following the switching off the Nd:YAG laser, is less than 1 s. These fast heating/cooling rates are achievable due to the method of direct heating of the wafer with the laser, and they likely represent the ultimate rates achievable with any RTA technique. The calculated transient temperature (broken line) describes reasonably well the dynamics of the process. The absolute values of calculated temperatures depend on the emissivity value (ε) of the wafer. For the case discussed in Fig. 2(a), we used $\varepsilon_{Si} = 0.7$, in agreement with reported data for Si at this temperature range [27]. Further verification of the accuracy of FEM-based modeling was provided by studying the Laser-RTA of InP wafers. Figure 2(b) shows transient temperature behavior at the center of the InGaAsP/InP wafer (sample #2) that was backside irradiated with the LD

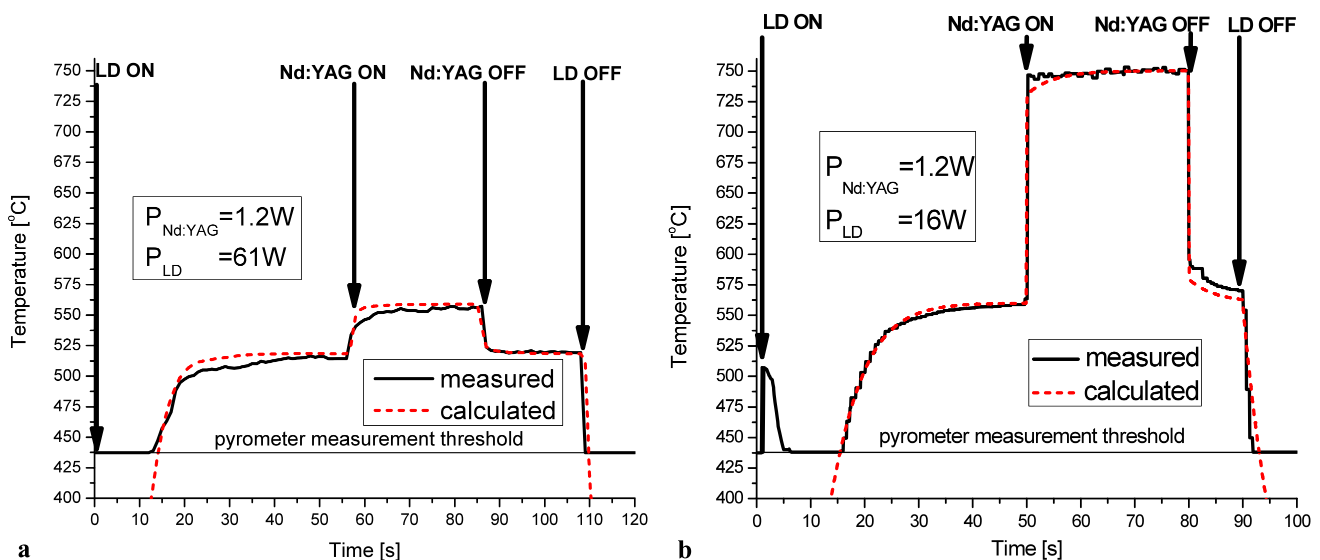

Fig. 2 Transient temperature behavior at the center of (**a**) Si wafer irradiated with a CW Nd:YAG laser at 1.2 W and backside heated with the 61 W radiation from a CW 980 nm laser diode, and (**b**) InP wafer comprising InGaAs/InGaAsP QW heterostructures irradiated with a CW Nd:YAG laser at 1.2 W and backside heated with the 16 W radiation from a CW 980 nm laser diode. Experimental and calculated results are shown by the *solid* and *broken lines*, respectively

to increase its temperature to 560°C. In this case, we used $\varepsilon_{InP} = 0.7$, which is greater than the emissivity of bulk InP reported in the literature [28]. Such an assumption, however, seems justified given the observed drastic reduction of the reflected power from InGaAsP/InP wafer following its coating with the SiO_2 layer. Note that achieving the same background temperature of the InGaAsP/InP wafer as that of the Si wafer required only 16 W of the LD power. Experimental results (solid line) show that this temperature is reached approximately 35 s from the onset of the irradiation. Additional irradiation with a 1.2 W Nd:YAG laser, at the 50th second of the experiment, resulted in a rapid increase of the temperature to 750°C. This temperature transition is achieved in less than 1 s, which is primarily due to the lower heat conductivity (dissipation) of InP in comparison to that of Si. The contribution of the SiO_2 layer to this behavior is marginal as its heat conductivity is significantly smaller than that of the InP wafer. The rapid temperature decrease (150 deg in less than 1.5 s) that is observed in this case, is comparable to the cooling rate of Si wafer. It can be seen that the FEM model (broken line) provides a reasonable description of measured transient temperatures.

For both Si and InGaAsP/InP wafers, the measured background temperatures stabilize at slightly slower rates than those predicted by the calculations. The likely reason for this discrepancy is the insufficient thermal isolation of wafers. However, it is clear that our model describes quite well the dynamics of the laser heating and cooling processes in Si and InGaAsP/InP wafers.

4 Quantum well intermixing in InGaAsP/InP microstructures

4.1 Temperature profiles

Figure 3 shows temperature profiles along the longer axis of the InP sample induced with a 41 W LD and a moving spot (0.5 mm) of the 1.2 W Nd:YAG laser. The results have been plotted for scans repeated in one direction (Fig. 3(a)) and two directions (Fig. 3(b)). A one-direction scan indicates that one of the sample edges will be underheated, while the other overheated. Scanning in two directions will result in a more uniform average temperature in the center of the sample. Therefore, we chose the two-direction scan mode in our study of the QWI process in sample #3.

4.2 Experimental results

Figure 4 presents the results of Laser-RTA for sample #3. The sample temperature was maintained at 620°C with the LD delivering 40 W to a 25 mm diameter spot. Five lines of the QWI material have been written sequentially with the Nd:YAG laser delivering 1.2 W power to a 0.5 mm diameter spot. The scanning speed of the spot was 1 mm/s. A PL map of the 2.5 mm × 10 mm fragment of the processed sample is shown in Fig. 4(a). Five lines of the QWI material, blue-shifted by approximately 15 nm, can easily be distinguished from the background of the as-grown material emitting at 1552 nm. Each line was fabricated following 20 double passes, which approximately corresponds to the dwell time of 20 s. We note that the same magnitude of the blueshift for this material, if background heated to 550°C,

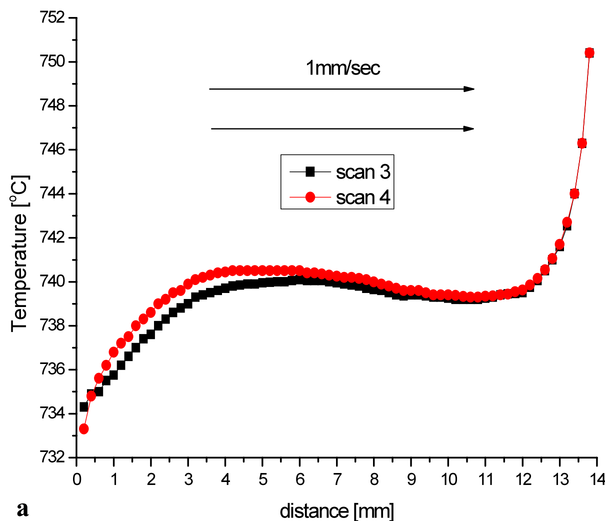

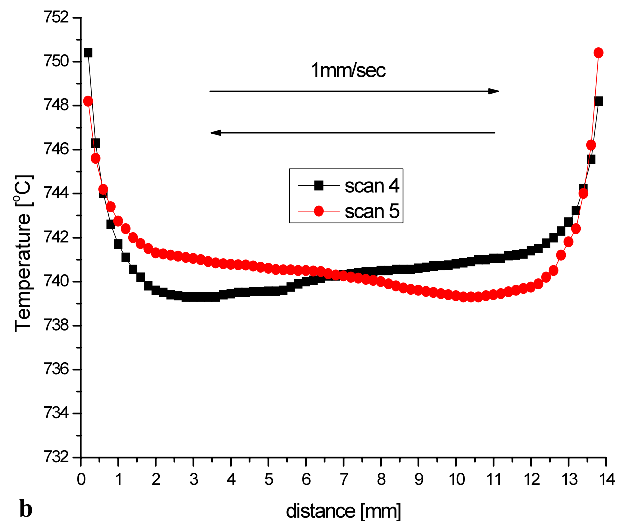

Fig. 3 Temperature profiles along the center of an InP sample induced with the 41 W 980 nm LD (24 mm diameter spot) and a spot (0.5 mm) of the 1.2 W Nd:YAG laser moving in one direction (**a**), and in two directions (**b**)

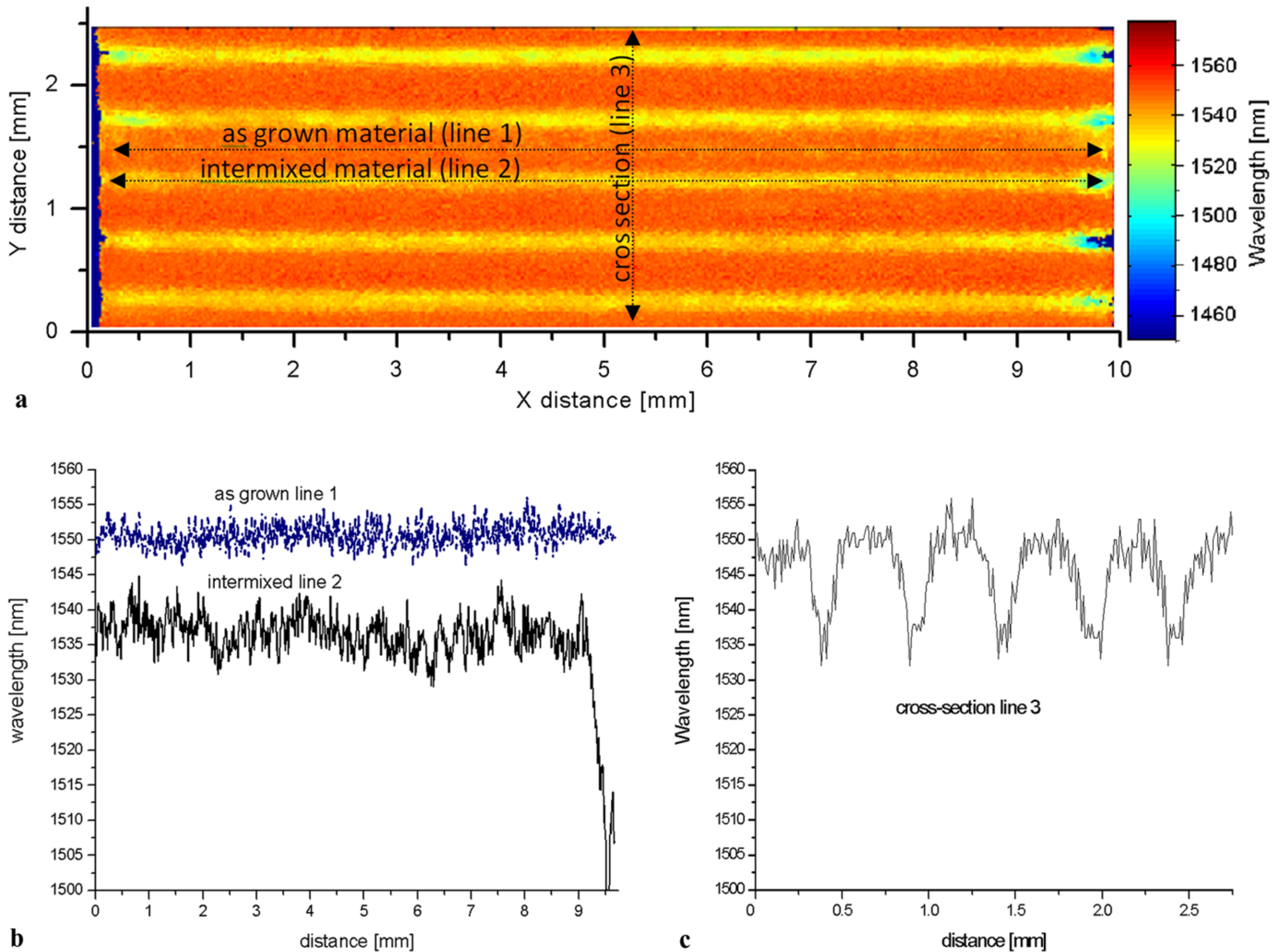

Fig. 4 Photoluminescence map of a Laser-RTA processed InGaAsP/InP QW sample with 5 lines of the intermixed material (**a**), photoluminescence peak position along the as-grown material, line 1, and the Laser-RTA produced line 2 of the intermixed material (**b**), and photoluminescence peak position across the sample (**c**)

required approximately a 30 s dwell time [30]. The significantly shorter dwell time in the current experiment indicates greater temperature achieved in the center of the Nd:YAG laser spot. The lines of the QWI material written in this experiment are approximately 300 μm wide, which indicates that only the top portion of the Nd:YAG Gaussian beam induced a temperature exceeding the threshold value for QWI. A comparison between PL peak position along the as-grown material (line 1) and the Laser-RTA produced line (line 2) is shown in Fig. 4(b). The PL peak position in the middle of the QWI line is 1538 ± 5 nm, which compares to 1552 ± 4 nm for the scan across the as-grown material. As predicted by the FEM calculations (Fig. 3(b)), both edges of the sample have been overheated and show the increased blue-shift amplitude of the QWI material. We expect that the effect of overheating the sample edges could be avoided by using a variable speed Nd:YAG laser beam. A cross-section PL scan across the processed sample is shown in Fig. 4(c). The maximum blue-shifted amplitudes that have been observed for each line of the QWI material are at 1535 ± 1 nm. This illustrates that the Laser-RTA technique achieves excellent reproducibility of the annealing conditions.

For the InGaAs/InGaAsP QW heterostructures, we have already reported blueshifts in excess of 220 nm [29]. As an illustration of the potential of the Laser-RTA technique in writing arbitrary contours of the QWI material, we show in Fig. 5 a PL map of the sample #4 that was irradiated with the GS controlled position of the Nd:YAG laser beam writing a letter "S". This 'watermark' was obtained following 400 passes of the 1.2 W Nd:YAG spot moving at 50 mm/s (4 s dwell time). The background temperature of the sample during this experiment was maintained at 620°C. It can be seen that the material has been intermixed uniformly along the entire S line with the contrast (blue shift of the bandgap) of approximately 10 nm. It is interesting to note that the width of this Laser-RTA written line is 100 μm,

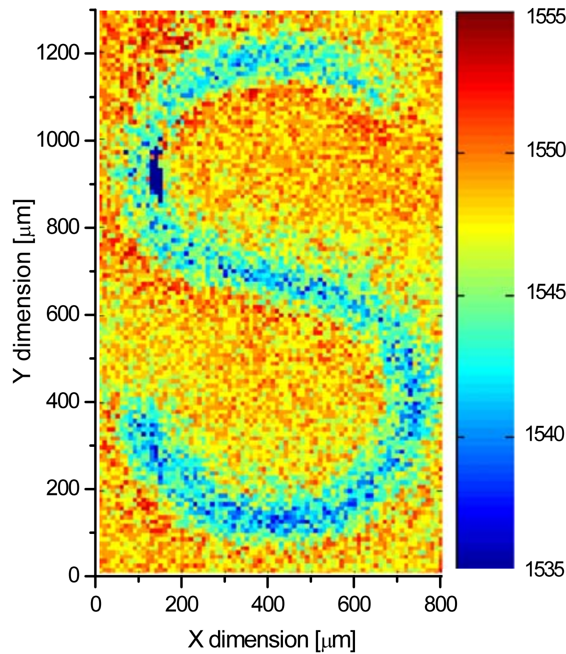

Fig. 5 Photoluminescence map of the Laser-RTA processed InGaAsP/InP QW ample with a 'watermark' of the QWI material

which is 5 times smaller than the diameter of the writing beam. This clearly demonstrates that similarly to the results discussed in Fig. 4, only the top portion of the Nd:YAG beam induced a temperature exceeding the threshold for QWI.

5 Conclusions

We have developed an innovative Laser Rapid Thermal Annealing (Laser-RTA) technique for selective area intermixing of QW wafers. The approach is based on the application of a 150 W 980 nm LD and a 30 W TEM00 Nd:YAG laser for simultaneous heating of the back and front sides of the wafer, respectively. The Laser-RTA technique generates heating rates of semiconductor wafers significantly exceeding those achieved with conventional RTA techniques. The dynamics of the Laser-RTA process and the ability to anneal arbitrary shape patterns, e.g., lines and circles, are well described using 3D FEM approximation and a commercial software. We have investigated the Laser-RTA technique for QWI of InGaAsP/InP QW microstructures. With a Nd:YAG laser beam focused to 0.5 mm, an array of 5 lines of the QWI material with its bandgap blue shifted by 15 nm has been successfully fabricated in a 10 mm × 14 mm sample. Each line of the QWI material is approximately 300 µm wide. We have illustrated the potential of the Laser-RTA technique in writing arbitrary contours of the QWI material by fabricating a 'watermark' (a letter "S") in the InGaAsP/InP QW microstructure. It is expected that the Laser-RTA technique will find applications in fine tuning of the emission wavelength at selected areas of quantum well and quantum dot wafers.

Acknowledgement Funds for this research have been provided by the Natural Sciences and Engineering Research Council of Canada. JJD is a Canada Research Chair in Quantum Semiconductors.

References

1. E.H. Li, *Quantum Well Intermixing for Photonics, SPIE Selected Papers* (SPIE, Bellington, 1998)
2. J.J. Dubowski, C.Nì. Allen, S. Fafard, Appl. Phys. Lett. **77**(22), 3583 (2000)
3. J.J. Dubowski, X.R. Zhang, X. Xu, J. Lefebvre, Z. Wasilewski, Proc. SPIE **5339**, 93 (2004)
4. J.H. Marsh, Semicond. Sci. Technol. **8**, 1136 (1993)
5. N. Holonyak, IEEE J. Sel. Top. Quantum Electron. **4**, 584 (1998)
6. O.P. Kowalski, C.J. Hamilton, S.D. McDoughall, J.H. Marsh, A.C. Bryce, R.M. De La Rue, B. Vögele, C.R. Stanley, Appl. Phys. Lett. **72**, 581 (1998)
7. P.J. Poole, G.C. Aers, Y. Feng, E.S. Koteles, R.D. Goldberg, I.V. Mitchell, IEEE Photonics Technol. Lett. **8**, 1145 (1996)
8. H. Kim, J.W. Park, D.K. Oh, K.R. Oh, S.J. Kim, I. Choi, Semicond. Sci. Technol. **15**, 1005 (2000)
9. J.D. Ralston, A.L. Moretti, R.K. Lain, F.A. Chambers, Appl. Phys. Lett. **50**, 1817 (1987)
10. J.E. Epler, R.D. Burnham, R.L. Thorn-ton, T.L. Paoli, M.C. Bashaw, Appl. Phys. Lett. **49**, 1447 (1986)
11. J.H. Marsh, A.C. Bryce, R.M. De La Rue, C.J. McLean, A. McKee, G. Lullo, Appl. Surf. Sci. **106**, 326 (1996)
12. B.S. Ooi, T.K. Ong, O. Gunawan, IEEE J. Quantum Electron. **40**, 481 (2004)
13. J.H. Marsh, O.P. Kowalski, S.D. McDougall, B.C. Qiu, A. McKee, C.J. Hamilton, R.M. De La Rue, A.C. Bryce, J. Vac. Sci. Technol. A **16**, 810 (1998)
14. P. Baumgartner, W. Wegscheider, M. Bichler, G. Schedelbeck, R. Neumann, G. Abstreiter, Appl. Phys. Lett. **70**, 2135 (1997)
15. J.J. Dubowski, C.Y. Song, J. Lefebvre, Z. Wasilewski, G. Ares, H.C. Liu, J. Vac. Sci. Technol. A **22**(3), 887 (2004)
16. A. Rastelli, A. Ulhaq, S. Kiravittaya, L. Wang, A. Zrenner, O.G. Schmidt, Appl. Phys. Lett. **90**, 073120 (2007)
17. C.K. Chia, S.J. Chua, J.R. Dong, S.L. Teo, Appl. Phys. Lett. **90**, 061101 (2007)
18. R. Stanowski, O. Voznyy, J.J. Dubowski, J. Laser Micro/Nanoengineering **1**(1), 17 (2006)
19. O. Voznyy, R. Stanowski, J.J. Dubowski, J. Laser Micro/Nanoengineering **1**(1), 48 (2006)
20. O.C. Zienkiewicz, R.L. Taylor, *The Finite Element Method*, 5th edn., vol. 1 (Academic Press, San Diego, 1996)
21. M.W. Steen, *Laser Material Processing*, 2nd edn. (Springer, Berlin, 1998)
22. V. Palankovski, R. Schulteis, S. Selberherr, IEEE Trans. Electron Dev. **48**, 1264 (2001)
23. W.J. Turner, W.E. Reese, G.D. Pettit, Phys. Rev. **136**, A1467 (1964)
24. D.E. Aspnes, A.A. Studna, Phys. Rev. B **27**, 985 (1983)
25. E.J. Skogen, Ph.D. Dissertation, http://www.ece.ucsb.edu/Faculty/Coldren/Dissertations/Skogen_Thesis.pdf

26. M. Beaudoin, A.J.G. DeVries, S.R. Johnson, H. Laman, T. Tiedje, Appl. Phys. Lett. **70**(26) (1997)
27. N.M. Ravindra, S. Abedrabbo, C. Wei, F.M. Tong, A.K. Nanda, A.C. Speranza, IEEE Trans. Semicond. Manuf. **11**(1), 30 (1998)
28. P.J. Timans, J. Appl. Phys. **72**, 660 (1992)
29. R. Stanowski, S. Bouaziz, J.J. Dubowski, Proc. SPIE **6879**, 68790D1-8 (2008)
30. Ioffe Physico-Technical Institute: http://www.ioffe.rssi.ru/SVA/NSM/Semicond
31. S.M. Sze, *Physics of Semiconductor Devices* (Wiley, New York, 1981)
32. C.J. Glassbrenner, G.A. Slack, Phys. Rev. **134**, A1058 (1964)